Available online at www.sciencedirect.com
SCIENCE DIRECT®
Nuclear Physics A 764 (2006) 261–273
NUCLEAR PHYSICS A

The ratio of proton electromagnetic form factors via recoil polarimetry at $Q^2 = 1.13$ (GeV/c)^2

G. MacLachlan [a,*], A. Aghalaryan [b], A. Ahmidouch [c], B.D. Anderson [d], R. Asaturyan [b], O. Baker [e], A.R. Baldwin [d], D. Barkhuff [f,1], H. Breuer [g], R. Carlini [h], E. Christy [e], S. Churchwell [i,2], L. Cole [e], E. Crouse [j], S. Danagoulian [h,b], D. Day [k], T. Eden [d,e,3], M. Elaasar [l], R. Ent [h], M. Farkhondeh [f], H. Fenker [h], J.M. Finn [j], L. Gan [e], K. Garrow [h], P. Gueye [e], C.R. Howell [i], B. Hu [e], M.K. Jones [h], J.J. Kelly [g], C. Keppel [e], M. Khandaker [m], W.-Y. Kim [n], S. Kowalski [f], A. Lai [d], A. Lung [h], D. Mack [h], R. Madey [d,h], D.M. Manley [d], P. Markowitz [o], J. Mitchell [h], H. Mkrtchyan [b], A.K. Opper [a], B. Plaster [f], C. Perdrisat [j], V. Punjabi [m], B. Raue [o], T. Reichelt [p], J. Reinhold [o], J. Roche [j], Y. Sato [e], N. Savvinov [g], A.Yu. Semenov [d], I.A. Semenova [d], W. Seo [n], N. Simicevic [q], G. Smith [h], S. Taylor [f], S. Stepanyan [b], V. Tadevosyan [b], S. Tajima [i], L. Tang [e], W. Tireman [d], P.E. Ulmer [r], W. Vulcan [h], J.W. Watson [d], S.P. Wells [q], F. Wesselmann [k], S. Wood [h], C. Yan [h], Chenyu Yan [d], S. Yang [n], L. Yuan [e], W.-M. Zhang [d], H. Zhu [k], X. Zhu [e]

[a] *Ohio University, Athens, OH 45701, USA*
[b] *Yerevan Physics Institute, Yerevan 375306, Armenia*
[c] *North Carolina A&T State University, Greensboro, NC 27411, USA*
[d] *Kent State University, Kent, OH 44242, USA*
[e] *Hampton University, Hampton, VA 23668, USA*
[f] *Massachusetts Institute of Technology, Cambridge, MA 02139, USA*
[g] *University of Maryland, College Park, MD 20742, USA*
[h] *Thomas Jefferson National Accelerator Facility, Newport News, VA 23606, USA*
[i] *Duke University and TUNL, Durham, NC 27708, USA*
[j] *The College of William and Mary, Williamsburg, VA 23187, USA*
[k] *University of Virginia, Charlottesville, VA 22904, USA*
[l] *Southern University at New Orleans, New Orleans, LA 70126, USA*
[m] *Norfolk State University, Norfolk, VA 23504, USA*
[n] *Kyungpook National University, Taegu 702-701, South Korea*
[o] *Florida International University, Miami, FL 33199, USA*
[p] *Rheinische Freidrich-Wilhelms-Universität, D-53115 Bonn, Germany*

0375-9474/$ – see front matter
doi:10.1016/j.nuclphysa.2005.09.012

[q] Louisiana Tech University, Ruston, LA 71272, USA
[r] Old Dominion University, Norfolk, VA 23529, USA

Received 18 May 2005; received in revised form 14 September 2005; accepted 16 September 2005

Available online 29 September 2005

Abstract

Recoil polarimetry was used to extract the ratio of the proton electromagnetic form factors, $\mu_p G_E^p / G_M^p = 0.878 \pm 0.064(\text{stat}) \pm 0.012(\text{sys})$, at $Q^2 = 1.13$ $(\text{GeV}/c)^2$ from the reaction $^1\text{H}(\vec{e}, e\vec{p})$. This was an ancillary measurement in which the proton polarization was determined as part of a larger program utilizing a stand-alone polarimeter designed to measure $\mu_n G_E^n / G_M^n$. This measurement complements previous recoil polarimetry measurements of $\mu_p G_E^p / G_M^p$ made at the Thomas Jefferson National Accelerator Facility.

PACS: 14.20.Dh; 13.40.Gp; 25.30.Bf; 24.70.+s

Keywords: NUCLEAR REACTIONS ^{1}H(polarized $e, e'p$), $E = 2329$ MeV; measured recoil proton spectra, polarization. ^{1}H deduced ratio of electromagnetic form factors.

1. Introduction

Much attention has recently been given to the proton electromagnetic form factors because of the apparent inconsistency in results [1] obtained from the Rosenbluth separation [2–4] and polarization transfer [5–7] measurements. Data taken with the Rosenbluth separation technique indicate that G_E^p and G_M^p have the same approximate Q^2 dependence, up to an overall scale factor, such that

$$\frac{\mu_p G_E^p(Q^2)}{G_M^p(Q^2)} \approx 1, \tag{1}$$

where μ_p is the proton magnetic moment. More recent polarization transfer measurements performed in Hall A at the Thomas Jefferson National Accelerator Facility reveal a linear deviation toward smaller values of the ratio G_E^p / G_M^p with increasing Q^2. It has been suggested [8] that this result indicates that the electric charge distribution of the proton may be more diffuse than previously thought, but in light of recent theoretical efforts [9,10] to understand the role of two-photon exchange contributions to elastic e–p scattering, a different physical description of the proton's

* Corresponding author. Current address: New Mexico State University, Department of Physics, Las Cruces, NM 88033, USA.

E-mail address: maclach@jlab.org (G. MacLachlan).

[1] Current address: Renaissance Technologies, 600 Route 25A, East Setauket, NY 11733, USA.

[2] Current address: Dept. of Physics and Astronomy, University of Canterbury, Private Bag 4800, Christchurch 8020, New Zealand.

[3] Current address: Atmospheric Chemistry Division, National Center for Atmospheric Research, Boulder, CO 80307, USA.

radial distribution of charge and magnetism may be forthcoming. A linear fit to the polarization transfer data taken in Hall A [6] gives the following result,

$$\mu_p g = 1.0 - 0.13\big(Q^2 - 0.4\big), \tag{2}$$

where

$$g \equiv \frac{G_E}{G_M}. \tag{3}$$

The Sachs form factors, G_E and G_M, describe the electric and magnetic structure of the nucleon and depend only on the transferred four-momentum squared, Q^2.

In the Rosenbluth separation technique a reduced cross section, σ_R, is defined as

$$\sigma_R = \frac{d\sigma}{d\Omega}\frac{\epsilon(1+\tau)}{\tau\sigma_{\mathrm{NS}}} = G_M^2 + \frac{\epsilon}{\tau}G_E^2, \tag{4}$$

where $\epsilon = [1 + 2(1+\tau)\tan^2(\theta/2)]^{-1}$ parametrizes the transverse component of the virtual photon polarization, θ is the scattering angle of the electron in the laboratory frame, $\tau = Q^2/4m_p^2$, and the "nonstructure" cross section, σ_{NS}, is expressed in terms of the incident beam energy, E, scattered electron energy E', and Mott cross section, σ_{Mott} as

$$\sigma_{\mathrm{NS}} = \frac{E'}{E}\sigma_{\mathrm{Mott}}. \tag{5}$$

In this method data are taken at a fixed value of Q^2, and consequently a fixed value of τ, while ϵ is varied by adjusting the beam energy and scattering angle. The magnetic form factor is extracted at $\epsilon/\tau = 0$; the electric form factor is extracted as the slope of the reduced cross section while ϵ/τ is varied. Because the electric form factor is suppressed by the factor ϵ/τ in the reduced cross section, G_E becomes increasingly difficult to extract at high momentum transfer.

Polarization transfer techniques use recoil polarimetry to measure the ratio of the sideways and longitudinal polarization components, P_S/P_L, of the recoil nucleon. In the plane-wave impulse approximation, the ratio of polarization components is proportional to the ratio of the electric and magnetic form factors [11],

$$\frac{P_S}{P_L} = -\frac{K_S}{K_L}g, \tag{6}$$

where K_S and K_L are functions of kinematic quantities τ and θ. As it is a ratio technique, polarization transfer methods do not suffer from the same systematic uncertainties as the Rosenbluth separation. The polarization measured is given by $P_i = \xi_i/A_{\mathrm{POL}}$, where P_i indicates a polarization component transverse to the nucleon's momentum, ξ_i the associated scattering asymmetry, and A_{POL} the effective analyzing power of the polarimeter. Because the polarization recoil technique measures a ratio, many systematic effects cancel. The polarimeter analyzing power and incident beam polarization need not be determined so long as they can be held constant. Also, physical differences in the polarimeter cancel in the cross ratio calculation of the asymmetries. Furthermore, there is no need to vary the beam energy or scattering angle, both of which are potential sources of systematic uncertainties in the Rosenbluth separation method.

We present the result of a polarization transfer measurement of G_E^p/G_M^p using a technique that differs from that used in Hall A. This experiment utilized a polarimeter designed specifically for this measurement while the Hall A measurement used a polarimeter in the focal plane of a magnetic spectrometer. This measurement was part of experiment 93-038, which was designed to measure the ratio of the electric and magnetic form factors of the neutron [12]. This result

provides an independent consistency check of the Hall A results and demonstrates the utility of the present technique for measuring the ratio of electromagnetic form factors.

2. The experiment

The experiment was performed at Jefferson Lab in Hall C with a longitudinally polarized 2329 MeV electron beam of 65 μA, and an unpolarized 15-cm liquid hydrogen target. The helicity of the incident beam was flipped at 30 Hz to minimize the effects of systematic differences with time scales longer than the flipping frequency, such as possible differences in the accumulated charge of each helicity state. The electron beam was scattered elastically from the LH_2 target and the scattered electrons were detected by the High Momentum Spectrometer (HMS) positioned at 30.82°. The HMS provided information about the momentum of the scattered electrons as well as timing signals that were used as part of the event trigger. Data from the HMS Čerenkov counter identified electrons and pions. The polarization of the incident electron beam was measured at regular intervals throughout the experiment with the Hall C Møller polarimeter.

2.1. Polarimeter

The recoil protons were detected with a polarimeter (NPOL), positioned at 46.0°, specifically designed for this experiment to measure the up-down scattering asymmetry arising from a transverse polarization. NPOL comprised a front array, a rear array, and front and rear taggers, shown schematically in Fig. 1. The front array acted as the analyzer for the polarimeter and consisted of twenty 10-cm × 10-cm × 100-cm scintillators arranged in four vertical layers, each stacked five scintillators high. The rear array was subdivided into two symmetric upper and lower arrays, each composed of three layers of four scintillators. The dimensions of the inner two scintillators of each layer of the rear array were 25.4-cm × 10.16-cm × 101.6-cm while the outer two were 50.8-cm × 10.16-cm × 101.6-cm. The front and rear taggers sandwiched the front array and were used for charged particle identification. The front taggers were arranged in two vertical layers, each composed of five thin (0.635-cm) scintillators stacked edgewise. The rear taggers were arranged into a single vertical layer composed of eight thin (0.635-cm) scintillators stacked edgewise.

NPOL was enclosed in a concrete hut with a steel collimator facing the target. The steel collimator was designed primarily to attenuate neutrons originating at the target and prevented

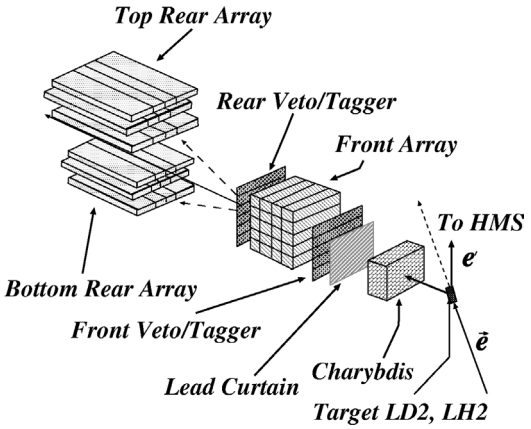

Fig. 1. Schematic diagram of polarimeter (NPOL).

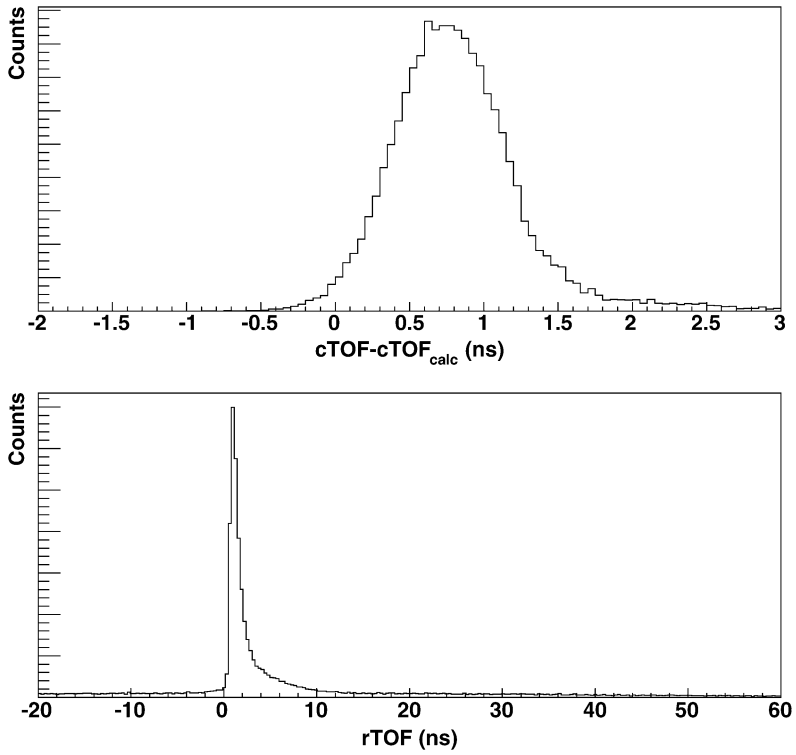

Fig. 2. Top panel: corrected time-of-flight spectrum comparing the difference between measured and predicted times-of-flight between the target and the front array. Bottom panel: front-rear array time-of-flight spectrum.

them from reaching the rear arrays. This collimator assured that protons originating at the target and recording signals in both front and rear arrays, underwent a rescattering in the front array. A 10-cm thick lead curtain whose purpose was to attenuate high energy photons and low energy charged particles from the target was situated upstream of the steel collimator.

2.2. Data analysis and calibration

The measured time-of-flight from the target to the front array (cTOF) was compared to a calculated time-of-flight, which was computed by assuming elastic scattering and using the electron kinematics determined by the HMS. A time-of-flight difference distribution, cTOF-cTOF$_{calc}$, is shown in the top panel of Fig. 2. The peak in Fig. 2 does not fall at zero because the calculated time-of-flight did not account for energy loss in the 10-cm thick lead curtain and detectors of the front array. The result is an offset to the corrected time-of-flight. A set of selection cuts was placed on the corrected time-of-flight from 0.0 to 1.5 ns so that only events falling within this range were used in the asymmetry calculation.

The scattering asymmetries, ξ, were determined from time-of-flight spectra (rTOF) between the front and rear arrays of NPOL. The parameter rTOF was normalized to a 250 cm flight path so that

$$\text{rTOF} \longrightarrow \text{rTOF}\left(\frac{250}{d}\right), \tag{7}$$

where d is the actual flight path length determined from the distance from the scattering vertex in the front array to the point of interaction in the rear array. The rTOF spectra were sorted by beam helicity and up-down scattering; a selection cut from -1.0 to 8.0 ns was placed on rTOF so that only events falling within this range were used to calculate the yields, which were used in determining the scattering asymmetry and discussed in the next subsection. A sample rTOF spectrum is shown in the bottom panel of Fig. 2. The signal-to-background ratio for these spectra was typically between 17 and 20 and a flat background was assumed and subtracted to obtain the scattering yields.

The polarimeter was calibrated for position and timing information. The front array left–right position calibration was performed by using proton data with Charybdis set at ± 80 A. At this setting the deflection of the protons forced the position spectra to be clipped thus determining the physical edge of the detector. The rear detector position calibrations were performed in a similar manner but with a range of Charybdis settings used to increase the number of events in the calibration. The tagger detectors were not illuminated across their entire length because of blocking by the steel collimator so the position calibration for the taggers was made by comparing against hits recorded in the front array.

The timing signals from each of the detectors in the front [rear] array were calibrated with respect to each of the other detectors in the front [rear] array. To eliminate difficulties arising from multi-hit events, the calibration was done with only single hit events. Events from $d(\vec{e}, ne)p$ in which the neutron was detected in NPOL were used for this calibration since the low detection efficiency of neutrons gave a sufficient number of events with a single hit in the front array and a single hit in the rear array. The timing calibration between the polarimeter and the HMS was performed by comparing predicted and measured time-of-flight distributions for neutron data and centering the difference at zero.

2.3. Ratio method

The scattering asymmetry, ξ, was determined from the number of helicity-wise events scattering upward or downward in NPOL. The label RU indicates an event in which an upward scattering occurred from a right-handed beam helicity state, and so forth for the other three possibilities. The yields for each possibility were combined to form the cross ratio, r, such that

$$r = \left[\frac{N_{LD}N_{RU}}{N_{LU}N_{RD}}\right]^{1/2}, \tag{8}$$

and the scattering asymmetry was given by

$$\xi = \frac{1-r}{1+r}. \tag{9}$$

The cross ratio technique cancels physical differences between the top and bottom rear arrays to all orders.

The sideways component of polarization for the recoil proton, P_S, is related to the measured asymmetry by

$$\xi = A_{\mathrm{POL}} P_S. \tag{10}$$

A measurement of both the sideways and longitudinal polarization components is necessary to extract the ratio of form factors as can be seen in Eq. (6). A vertical dipole magnet, Charybdis, was positioned upstream of NPOL to precess the proton polarization about the vertical axis

and mix P_S and P_L. The polarization was precessed by an angle, χ^+, and the resulting asymmetry, $\xi_{+'}$, was measured. Then the Charybdis field was reversed to give an equal but opposite precession angle, χ^-, and the corresponding asymmetry, $\xi_{-'}$, was also measured. A ratio of asymmetries, $\eta \equiv \xi_{-'}/\xi_{+'}$, was used along with Eq. (10) to give

$$\eta \equiv \frac{\xi_{-'}}{\xi_{+'}} = \frac{A^-_{\mathrm{POL}}}{A^+_{\mathrm{POL}}} \frac{P^-_S}{P^+_S}, \tag{11}$$

where $P_S^{+(-)}$ was the sideways component of polarization after precession by the angle $\chi^{+(-)}$ and $A^{+(-)}_{\mathrm{POL}}$ represents the polarimeter analyzing power during a precession by $\chi^{+(-)}$. Because protons are electrically charged they experienced a deflection while inside the magnetic field of Charybdis. This effect limited the Charybdis field strength that could be used for the measurement because an excessively strong field would steer the protons away from the polarimeter. In a simple dipole field the precession angle is related to the deflection angle by $\chi = \gamma(\mu_p - 1)\phi$ where γ is the usual relativistic factor, μ_p is the magnetic moment of the proton, and ϕ is the deflection angle. The HMS and NPOL acceptances limited ϕ to approximately $\pm 2.8^\circ$ and consequently the precession angles, $\chi^\pm$ were limited to $\pm 8.3^\circ$.

The sideways polarizations for each precession angle are related to the ratio of the transferred sideways and longitudinal polarization components by

$$\frac{P^-_S}{P^+_S} = \frac{(P_S/P_L)\cos\chi - \sin\chi}{(P_S/P_L)\cos\chi + \sin\chi}. \tag{12}$$

The ratio of form factors can then be expressed in terms of η and χ by inverting Eq. (12), using Eqs. (6) and (11), and assuming $A^+_{\mathrm{POL}} = A^-_{\mathrm{POL}}$ to within uncertainties. The resulting expression is

$$g = \frac{K_L}{K_S}\left(\frac{\eta + 1}{\eta - 1}\right)\tan\chi. \tag{13}$$

Systematic uncertainties associated with differences in A^+_{POL} and A^-_{POL}, as well as uncertainties in χ, are discussed in Section 3.

It is also important that the kinematics remain constant for data taken in both precession states. A narrow acceptance cut on the invariant mass, $W = m_p \pm 12$ MeV/c^2 where m_p is the proton mass, eliminated inelastic events and also those events in which bremsstrahlung radiation was emitted. In both cases these events appear in the high energy tail of W and were discarded. The invariant mass is related to Q^2 by

$$W = \sqrt{m_p^2 + 2m_p(E - E') - Q^2}. \tag{14}$$

Spectra for both W and Q^2 are shown for both positive and negative Charybdis polarities in Fig. 3. The mean for the invariant mass with positive [negative] Charybdis polarity is 0.9399 [0.9389] (GeV/c^2) with an RMS value of 0.0111 [0.0126] (GeV/c^2). The mean for the transferred four-momentum with positive [negative] Charybdis polarity is 1.119 [1.136] (GeV/c)^2 with an RMS value of 0.044 [0.044] (GeV/c)^2. The kinematics of the events used for the two phases of the experiment agree well with each other, within the statistical uncertainties.

2.4. Determination of G_E^p/G_M^p

An algorithm was used to determine η in which event-wise rather than averaged kinematics were used. The event-wise method made no assumptions about correlations between kinematic

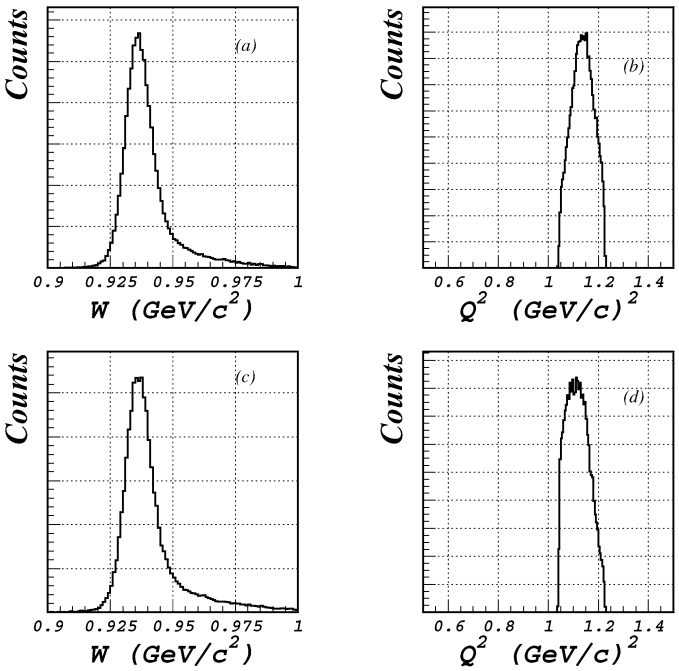

Fig. 3. Kinematics for both Charybdis polarities: (a) invariant mass for Charybdis with positive polarity. (b) Transferred momentum squared with positive polarity. (c) Invariant mass for Charybdis with negative polarity. (d) Transferred momentum squared with negative polarity. The plots of Q^2 are for events passing the W cut.

factors and precession angles as would be necessary if one used the mean values for the precession angles, $\bar{\chi}^{\pm}$, and kinematic factors, $\bar{K}_S$ and $\bar{K}_L$, in Eq. (13). In the event-wise method the kinematics for each detected proton were determined from the corresponding electron data obtained by the HMS, and both the sideways and longitudinal polarization components of the proton were calculated using Eq. (12) from Ref. [11] with the value for $g = G_E/G_M$ being set by the fit to the Hall A data, given in Eq. (2). We emphasize that the data themselves determined the kinematics and weighting; τ and θ_e were determined from the HMS data with the assumption of elastic scattering.

Any event-wise correlation between kinematic factors and precession angle is preserved in this approach. The event-wise method has an advantage over Monte Carlo methods in that it exploits the fact that the data themselves reflect the detector acceptances and resolution characteristics, as well as actual physical effects such as the τ and θ dependences of the differential cross section. After calculating the transferred polarization, the recoil proton was assigned a position and a momentum which were consistent with the HMS information and the assumption that the scattering was elastic. The precession and deflection for each proton passing the event selection were calculated along the path through Charybdis by integrating the classical equations of motion as described in Ref. [13].

Depolarization occurring from nuclear interactions within the 10-cm lead curtain were simulated by treating the lead as a Fermi gas and calculating the five helicity amplitudes necessary to describe NN scattering as described in Ref. [14]. The magnitude of the effect of depolarization on η is discussed in the section on uncertainties.

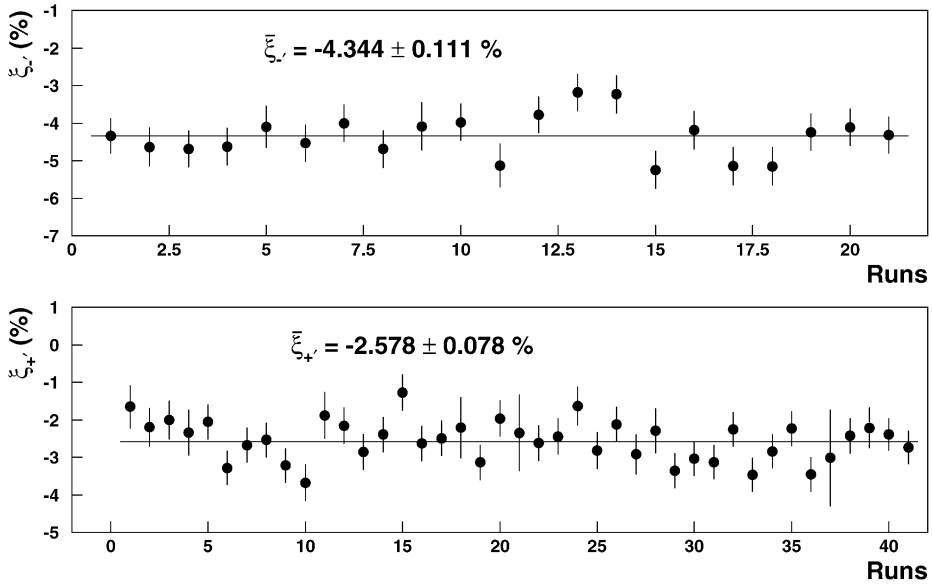

Fig. 4. Measured asymmetries for runs with negative [positive] Charybdis polarity shown in top [bottom] panel.

The ensemble averages of the sideways polarizations presented to NPOL for both Charybdis polarities were calculated thus and the ratio of the two was defined as

$$\eta_{\text{pre}} \equiv \frac{\bar{P}_S^-}{\bar{P}_S^+}, \tag{15}$$

where η_{pre} is equivalent to the predicted ratio of asymmetries which were compared to the measured ratio of asymmetries,

$$\eta_{\text{meas}} \equiv \frac{\bar{\xi}_{-'}}{\bar{\xi}_{+'}}. \tag{16}$$

Measured asymmetries were extracted from the data as in Eqs. (8)–(10); the results for each precession angle are shown in Fig. 4. The difference between the predicted and measured asymmetries was squared and an error-weighted difference-squared function,

$$\Delta^2 = \frac{[\eta_{\text{pre}}(\kappa) - \eta_{\text{meas}}]^2}{\sigma^2}, \tag{17}$$

was computed where σ represents the experimental uncertainties added in quadrature. This was repeated for nine assumed values of $G_E/G_M \to \kappa G_E/G_M$ where κ was a dimensionless scale factor such that

$$\kappa \in \{0.75,\ 0.875,\ 0.9,\ 0.95,\ 1.0,\ 1.05,\ 1.1,\ 1.175,\ 1.25\}.$$

The resulting nine values of $\Delta^2(\kappa)$ were fitted with a function whose minimum determined the value of κ that most closely matched the experimentally measured ratio, η_{meas}, and thereby determined G_E/G_M (see Fig. 5). The value of the parameter that minimized the fitting function was $\kappa = 1.023$.

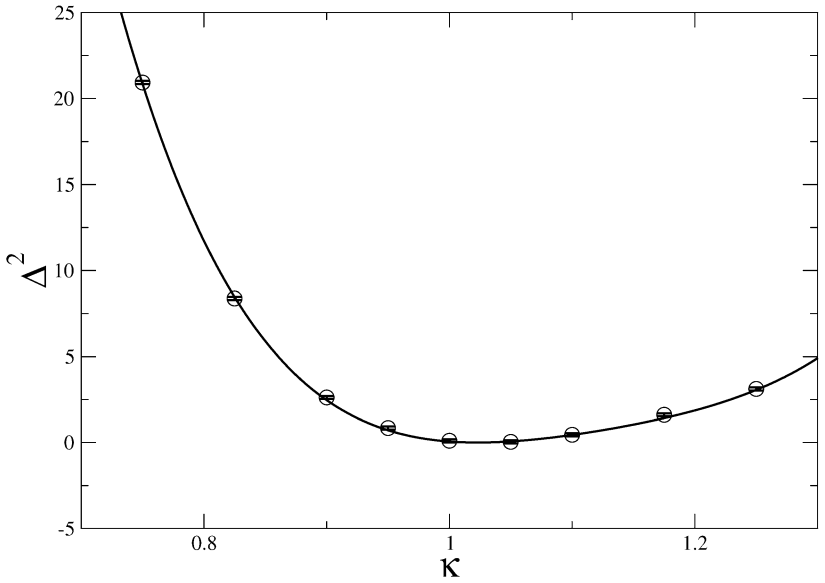

Fig. 5. Differences between measured and predicted ratio of asymmetries squared as a function of scale parameter κ. Circles indicate calculated differences and the fit to these points is shown as the solid line.

3. Systematic and statistical uncertainties

In all, 62 runs were used for the extraction of G_E^p/G_M^p, corresponding to about 6 Coulombs of charge on target. Of these data, 21 runs were with the Charybdis polarity in the $(-)$ state while 41 runs were used with Charybdis in the $(+)$ state. We note that the difference in number of runs for the $\pm$ Charybdis states was to account for the smaller component of the sideways polarization in the $(+)$ state.

The largest systematic uncertainties were associated with the determination of the beam polarization, the Charybdis field, and the timing calibration. The list of systematic and statistical uncertainties is given in Table 1. In this ratio technique, knowledge of the absolute beam polarization is unnecessary for extracting G_E/G_M so long as it remains constant over the run period. Uncertainties in G_E/G_M may arise from uncertainties in the beam polarization and in differences in the beam polarization during the two phases of the measurement. The measurement was carried out in approximately 30 hours and the beam polarization was measured three times during this period with a Møller polarimeter. The error weighted average of these measurements gives an average beam polarization of 72.20 $\pm$ 0.13%, with no apparent change over the time of the experiment. The effect of this polarization uncertainty on G_E/G_M was estimated to be 0.47%. Uncertainties and instabilities in the Charybdis field lead to related uncertainties in the precession angle, χ. Rather than treat these contributions to the uncertainty in χ collectively, we studied them on an individual basis and present the results as they effect the uncertainty in g. One source of uncertainty is the reliability of the magnetic field map generated from measurements of the Charybdis field. The other is the power supply for Charybdis which had 0.5% level fluctuations in the current it supplied ($\sim$ 50 A). The combined percent uncertainty in G_E/G_M from these two effects is 1.12%. The uncertainty from the NPOL timing calibration was estimated

Table 1
Error budget for G_E/G_M

	Uncert $\delta g/g$ [%]
Beam polarization	0.47
Charybdis power supply	0.51
Charybdis field map	1.01
Timing calibration	0.54
Traceback	0.17
HMS central momentum	< 0.06
Beam energy	< 0.03
Precession angle	< 0.01
Depolarization	< 0.01
Radiative corrections	< 0.10
Total systematic uncertainty	1.36
Total statistical uncertainty	7.26
Total uncertainty	7.39

by comparing the different physical asymmetries, $\xi_{\pm'}$ obtained from different choices of input calibration data.

Just as the beam polarization cancels, in principle, in the ratio P_S/P_L so does the NPOL analyzing power, A_{POL}, as long as it does not vary during measurements of the two precession angles. Analyzing powers were calculated for data sets with the two Charybdis polarities by calculating the sideways polarization presented to the polarimeter as described above, and combining this with the measured asymmetries and Eq. (10). The resulting analyzing powers were $A^{+}_{\mathrm{POL}} = 0.2250 \pm 0.0076$ and $A^{-}_{\mathrm{POL}} = 0.2210 \pm 0.0060$. Within the precision of this measurement, $A^{+}_{\mathrm{POL}} = A^{-}_{\mathrm{POL}}$ and they cancel each other in Eq. (11). Other systematic effects which contributed less significantly to the uncertainty of G_E/G_M include track reconstruction or traceback, the HMS central momentum, and the incident beam energy. The effect of depolarization on the ratio $\bar{P}^{-}_{S}/\bar{P}^{+}_{S}$ was estimated by simulating η with and without nuclear interactions. The magnitude of the depolarization effect on η is given in Table 1.

At the present time, a full calculation of radiative effects of polarization observables does not exist. Radiative corrections for *ep* scattering experiments that select events based on nucleon kinematics have been estimated by Afanasev et al. [17] using lowest order model independent corrections. On the basis of the work by Afanasev et al., we estimate the relative uncertainty of g due to radiative corrections to be less than 0.10%, as may be seen in Table 1.

The statistical uncertainty was related to the amount of data and resulted in an uncertainty of 7.26%. This was the largest contribution to the total uncertainty and corresponds to ≈ 6 C of charge on target or equivalently, ≈ 30 h of beam time.

4. Results and discussion

The ratio of the Sachs form factors for the proton was determined to be

$$\frac{\mu_p G_E}{G_M} = 0.878 \pm 0.065(\mathrm{stat}) \pm 0.011(\mathrm{sys}) \tag{18}$$

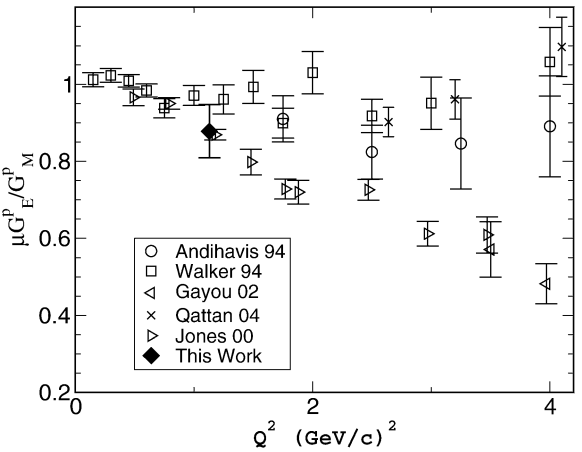

Fig. 6. Ratio of form factors extracted with the Rosenbluth separation technique shown as circles and squares [3,4]. SuperRosenbluth data shown as crosses [16]. Polarization transfer measurements are shown as triangles [5,6]. Result of this work is shown as a bold diamond.

at $Q^2 = 1.13\ (\mathrm{GeV}/c)^2$ using this polarization transfer technique. This result agrees well with the previous Hall A measurement as may be seen in Fig. 6. However, because of its large statistical uncertainty it lies within 1σ of the results from the Rosenbluth separation.

Presently, it is thought that two-photon corrections to radiative effects are responsible for at least some of the disagreement between the Rosenbluth separation and recoil polarimetry methods [9]. In particular, with two-photon exchange diagrams included, the cross section is modified by the virtual photon polarization, ϵ. The size of the two-photon effect has been studied with electron–proton and positron–proton elastic scattering at $Q^2 \leqslant 0.5\ (\mathrm{GeV}/c)^2$ [15] and a decrease to the cross section attributed to the two-photon corrections has been observed.

Estimates of the size of the two-photon contribution may possibly explain the disagreement between the Rosenbluth and recoil polarimetry techniques if the corrections for large-ϵ increases the cross section by approximately 6%, relative to small-ϵ corrections [16]. Consequently, the Rosenbluth data are sensitive to both one- and two-photon exchange because that extraction method relies on several cross section measurements over a range of ϵ. Recoil polarization measurements, being ratios of scattering yields at the same kinematics and ϵ, are less sensitive to ϵ dependent corrections. However, this explanation remains only conjecture until two-photon corrections are studied in detail at $Q^2 \geqslant 1\ (\mathrm{GeV}/c)^2$.

This measurement, with a stand-alone polarimeter, complements the Hall A measurement obtained with a focal plane polarimeter though statistical uncertainty makes it impossible to rule out the result obtained via the Rosenbluth separation technique without more data. However, this work suggests that this technique could be used successfully to determine $\mu_p G_E^p/G_M^p$ at $Q^2 > 1\ (\mathrm{GeV}/c)^2$. In addition, the result reported here also suggests the validity of the measurements of $\mu_n G_E^n/G_M^n$ using the same or similar polarimeter [12]. A proposal by our collaboration for an experiment employing an improved version of the polarimeter reported on here has been accepted at Jefferson Lab for a measurement of $\mu_n G_E^n/G_M^n$ at $Q^2 = 4.3\ (\mathrm{GeV}/c)^2$.

Acknowledgements

This work was supported in part by the National Science Foundation and the US Department of Energy. The Southeastern Universities Research Association (SURA) operates the Thomas Jefferson National Accelerator Facility under contract from the US Department of Energy.

References

[1] J. Arrington, Phys. Rev. C. 69 (2004) 022201.
[2] A.F. Sill, et al., Phys. Rev. D. 48 (1993) 29.
[3] R.C. Walker, et al., Phys. Rev. D. 49 (1994) 5671.
[4] L. Andivahis, et al., Phys. Rev. D. 50 (1994) 5491.
[5] M.K. Jones, et al., Phys. Rev. Lett. 84 (2000) 1398.
[6] O. Gayou, et al., Phys. Rev. Lett. 88 (2002) 092301.
[7] O. Gayou, et al., Phys. Rev. C. 64 (2001) 038202.
[8] J.J. Kelly, et al., Phys. Rev. C. 66 (2002) 065203.
[9] P.G. Blunden, W. Melnitchouk, J.A. Tjon, Phys. Rev. Lett. 91 (2003) 142304.
[10] Y.C. Chen, A. Afanasev, S.J. Brodsky, C.E. Carlson, M. Vanderhaeghen, Phys. Rev. Lett. 93 (2004) 122301.
[11] R.G. Arnold, C.E. Carlson, F. Gross, Phys. Rev. C. 23 (1981) 363.
[12] R. Madey, et al., Phys. Rev. Lett. 91 (2003) 122002.
[13] V. Bargmann, Louis Michel, V.L. Telegdi, Phys. Rev. Lett. 2 (1959) 435.
[14] C. Lechanoine-LeLuc, F. Lehar, Rev. Mod. Phys. 65 (2003) 47.
[15] J. Arrington, Phys. Rev. C 69 (2004) 032201.
[16] I.A. Qattan, et al., Phys. Rev. Lett. 94 (2005) 142301.
[17] A. Afanasev, I. Akushevich, N. Merenkov, Phys. Rev. D. 64 (2001) 113009.